Check for updates

Received: 19 January 2022 | Revised: 25 May 2022 | Accepted: 31 May 2022

DOI: 10.1002/ep.13925

ENVIRONMENTAL PROGRESS & SUSTAINABLE ENERGY

ORIGINAL RESEARCH

Remediation and Treatment

Influence of different Ag/ZnO heterostructures on the removal efficiency of multidrug-resistant *Enterococcus faecium* harboring multiple resistance genes from tap water

Eric T. Anthony[1,2,3] | **Mike O. Ojemaye**[1,2,3] | **Omobola O. Okoh**[1,2] | **Anthony I. Okoh**[2,3]

[1]Department of Pure and Applied Chemistry, University of Fort Hare, Alice, South Africa

[2]SAMRC Microbial Water Quality Monitoring Centre, University of Fort Hare, Alice, South Africa

[3]Applied Environmental Microbiology Research Group (AEMREG), University of Fort Hare, Alice, South Africa

Correspondence
Eric T. Anthony, Department of Pure and Applied Chemistry, University of Fort Hare, Alice 5700, South Africa.
Email: earl_ric@yahoo.com; 201927134@ufh.ac.za

Funding information
Govan Mbeki Research and Development Centre, University of Fort Hare, South Africa; South African Medical Research Council

Abstract

The adsorption efficiency of different Ag/ZnO heterostructures was investigated for the removal of multidrug-resistant *Enterococcus faecium* (MDR_*EF*) harboring multiple resistance genes from tap-water. The concentration of the precursors influences the microstructures of the adsorbents; however, it did not significantly affect the adsorption efficiency. The maximum adsorption capacity, q_e, (34.11 CFU/g), was obtained for $Ag_1Zn_{3.5}$. The kinetic studies revealed that Ag_1Zn_1 and Ag_1Zn_2 adsorbents agreed to the pseudo-first-order kinetic equation and adsorbents Ag_2Zn_1, $Ag_{3.5}Zn_1$ and $Ag_1Zn_{3.5}$ agreed to the pseudo-second-order kinetic equation. Initial tap-water pH range was beneficial for the adsorption and the pH of the treated tap-water was within the WHO tap water recommendation (6.5–8.5), whereas the effect of ionic strength, anionic and cationic interference was insignificant in the adsorption of MDR_*EF* onto the different heterostructure. Interestingly, the MDR_*EF* could retain its cell membrane integrity and resistance genes, suggesting that surface adsorption was the primary mechanism for the removal.

KEYWORDS
adsorption, Ag/ZnO heterostructures, antibiotic resistance bacteria, innersphere complexation

1 | INTRODUCTION

The ease of distributing multidrug-resistant bacteria (MDRB) and its impact on global socioeconomic proceedings have shifted attention toward its complete elimination from drinking water because this class of bacteria renders antibiotics ineffective in the fight against bacteria infection.[1] Drinking water represents the most vital route in which humans are exposed to MDRB.[2] Thus, the United Nations have been making tremendous efforts to reduce the number of deaths and illnesses associated with bacteria contamination through improved access to safe water.[3] However, recent reports have revealed that the conventional drinking water treatment plants (DWTP) are inadequate to eliminate MDRB from drinking water, and this has been attributed to the prevalence of MDRB in treated drinking water.[4]

The United Nations Children's Fund estimated that over 800 children die daily due to unclean water consumption (UNICEF, 2019). Pathogenic infection caused by the intake of contaminated drinking water is not only limited to low-budget countries. Among the common pathogens, *Enterococcus* is clinically essential. It persists in the environment,[5] and its presence in water is an indication of microbial pollution.[6] The presence of *Enterococci* is not permissible in drinking water in the European Union.[7] MDR *Enterococcus faecium* is considered the leading cause of healthcare-associated infection in the USA[8] and Germany.[9] The infection associated with *E. faecium* is vast and challenging to treat because this species is

 © 2022 American Institute of Chemical Engineers.

more antibiotic-resistant than *Enterococcus faecalis*. Thus, many *E. faecium* infected patients require intensive care.[10]

In other to reduce the infection caused by *E. faecium*, it is necessary to disinfect drinking water. The reactive species-based Advanced Water Treatment Technology (AWTT) has been considered one of the ultimate tools to tackle MDRB in the aqueous system, but the success is limited by incomplete disinfection. For example, Giannakis et al.[11] reported that streptomycin-resistant *Escherichia coli* regrowth after AWTT. Similarly, reactive radicals attack the cell membrane of MDRB and released the intracellular and extracellular genes that may expose resistance on bacteria cells.[12] In addition, the infrastructural setup has been one of the major setbacks for the implementation of AWTT, especially in low budget countries and rural communities. In place of this, Oladoja[13] proposed a decentralized onsite water treatment option for the attenuation of contaminated water in low-budget communities.

Adsorption-based approaches are among the decentralized methods that have been investigated to remove microbial contaminants in drinking water[14] because this technology restricts horizontal gene transfer associated with reactive species-based disinfection.[15] In lieu, graphene oxide was used to exclude *Staphylococcus aureus* in water,[16] BiOCl microspheres showed strong binding toward MDRB,[17] and dichalcogenides caused irreparable cell damage.[18] Meanwhile, adsorbents rich in silver and zinc have received tremendous attention.[19,20] In the dark, ZnO function by attaching to the bacteria cell wall without causing cell lysis.[21] Silver, a Lewis acid, have affinity for the sulfur and phosphorous, which are the significant components of cell wall/membrane[22]; thus, it also functions by physical contact with the bacteria, causing morphological changes[23] and bacteria inactivation.[24] However, gram-positive bacteria have shown resistance toward mechano-bactericidal action of nanostructures.[25]

The use of Ag/ZnO in water treatment has been gaining attention, especially as photocatalyst.[26,27] Ag/ZnO as photocatalyst have been used for the oxidation of phenolic compounds,[28] and dye stuffs.[29] Ag/ZnO decorated on carbon nanofibers was used for the oxidation of *E. coli*.[30]

This study reports the adsorption efficiency of different Ag/ZnO heterostructures, synthesized via the self-propagation combustion reaction, toward the gram-positive MDR *E. faecium*, harboring tetracycline and macrolides resistance genes. The thicker peptidoglycan layer (20–80 nm) would limit cell membrane breakage[31] due to the adsorbent mechanical mixing and subsequent adhesion with the MDR *E. faecium* harboring multiply resistance genes. The precursors were selected due to their bactericidal and bacteriostatic activities[32,33] and due to the significant difference in the ionic radii: Zn^{2+} (74 pm) and Ag^0 (144 pm)[34] to form a thermodynamically stable composite. The ratio of the precursors was also selected to gain an insight into how different dosage precursors induce the morphological assemblage of the resulting composite. The study focuses on removing MDR *E. faecium* from tap water, the determination of the influence of physicochemical properties of tap water on the removal efficiency, and the evaluation of the bacteria genetic integrities of resuscitated MDR *E. faecium* on adsorption.

2 | EXPERIMENTAL

2.1 | Materials and Methods

2.2 | Methods

2.2.1 | Synthesis of Ag/ZnO heterostructure

The Ag/ZnO were prepared via the self-propagating combustion protocol.[35] Briefly, different molar ratios (1:1, 2:1, 1:2, 3.5:1 and 1: 3.5) of $AgNO_3$ and $Zn(NO_3)_2{\cdot}6H_2O$ were dissolved in the presence of fixed molar concentration of urea, the solutions were calcined separately at 550°C for 30 min in a muffle furnace at an heating rate of 45°C/min, and labeled as Ag_1Zn_1, Ag_2Zn_1, Ag_1Zn_2, $Ag_{3.5}Zn_1$, $Ag_1Zn_{3.5}$, respectively. In this technique, NH_3 and $NO/NO_2/O_2$ were generated in situ and used as fuel and oxidant, respectively. The details of the adsorption experiment can be found in the Appendix S1. The reaction proceeds according to Equations (1–5):

$$2AgNO_{3(sol)} \rightarrow 2Ag_{(s)} + O_{2(g)} + 2NO_{2(g)} \quad (1)$$

$$Zn(NO_3)_2.6H_2O_{(sol)} \rightarrow ZnO_{(s)} + NO_{2(g)} + NO_{(g)} + O_2 + 6H_2O_{(g)} \quad (2)$$

$$NH_2 - CO - NH_{2(sol)} \rightarrow NH_{3(g)} + HNCO_{(g)} \quad (3)$$

$$HNCO_{(g)} + H_2O_{(g)} \rightarrow NH_{3(g)} + CO_{2(g)} \quad (4)$$

$$Ag_{(sol)} + ZnO_{(sol)} \rightarrow (Ag - ZnO)_s \quad (5)$$

3 | RESULT AND DISCUSSION

3.1 | XRD analysis of Ag/ZnO heterostructure

The XRD patterns are presented in Figure 1. The XRD pattern showed distinct and sharp peaks, suggesting a highly crystalline composite. The diffraction peaks in all the composites can be attributed to a mixed phase of Ag^0 (JCPDS 00-004-0783) and ZnO (JCPDS 00-036-1451). Using the Scherrer equation,[36] the average crystallinity size of the composites Ag_1Zn_1, Ag_2Zn_1, Ag_1Zn_2, $Ag_{3.5}Zn_1$, $Ag_1Zn_{3.5}$ were calculated to be 91.78, 29.84, 29.50, 26.54 and 29.64 nm, respectively.

3.2 | Point zero charge value

The results obtained for the point zero charge (PZC) are presented in Figure 2. The PZC is the pH in which the net charge on the surface of

19447450, 2022, 6, Downloaded from https://aiche.onlinelibrary.wiley.com/doi/10.1002/ep.13925 by South African Medical Research, Wiley Online Library on [22/02/2026]. See the Terms and Conditions (https://onlinelibrary.wiley.com/terms-and-conditions) on Wiley Online Library for rules of use; OA articles are governed by the applicable Creative Commons License

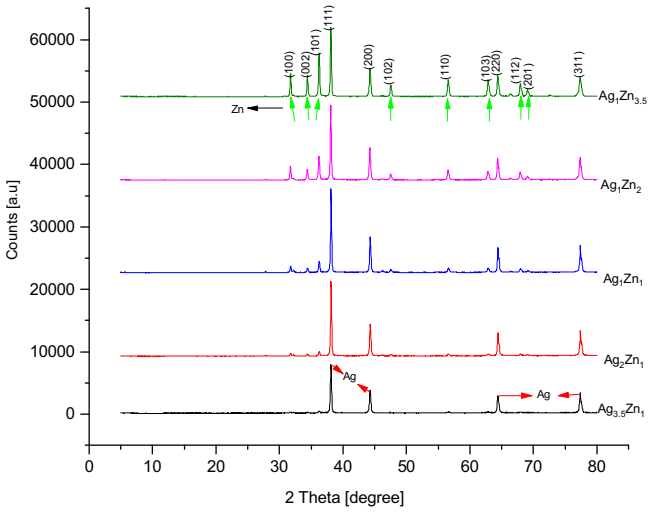

FIGURE 1 XRD pattern of Ag_1Zn_1, Ag_2Zn_1, Ag_1Zn_2, $Ag_{3.5}Zn_1$, and $Ag_1Zn_{3.5}$

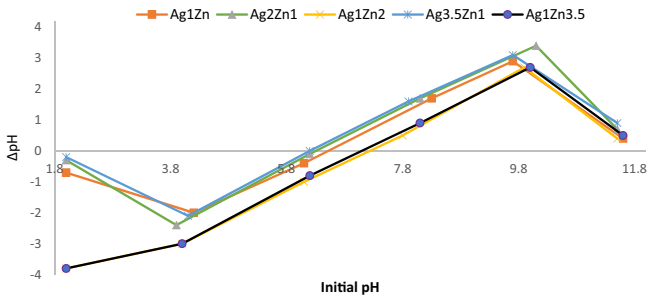

FIGURE 2 Point zero charge of the synthesized adsorbents

the adsorbent is equal to zero. Below the pH_{PZC}, the adsorbent surface is predominantly positively charged and above, it is predominantly negatively charged. The value of the PZC of Ag_1Zn_1, Ag_2Zn_1, Ag_1Zn_2, $Ag_{3.5}Zn_1$, $Ag_1Zn_{3.5}$ are 6.6, 6.3, 7.3 6.2, 7.1, respectively. The PZC of all the adsorbents followed a pattern. At higher Ag^+ ions dosage, the PZC was below pH 6.3, at higher Zn^{2+} ion dosage, the PZC was above pH 7.3, while at even precursors dosage, the PZC lies at pH 6.6. This implies that the amount of precursor in the synthesized adsorbents, affects the positive and negative charge distribution on the surface of the adsorbent.

3.3 | FTIR of Ag/ZnO heterostructures

The synthesized Ag/ZnO heterostructures were analyzed using FTIR in the range 4000–400 cm^{-1}. The results are presented in Figure 3. The analysis showed a minor peak at 3740 cm^{-1}, which is attributed to O—H stretching[37] or could also be likened to Ag—O—H; this peak is peculiar to $Ag_{3.5}Zn_1$ and Ag_2Zn_1, it was absent in $Ag_1Zn_{3.5}$ and Ag_1Zn_2 as the dosage of Zn^{2+} precursor increased. All other peaks were displayed in the fingerprint region of the IR, suggesting a highly pure sample. The peak at 418 cm^{-1} is characterized by Ag,[38] and

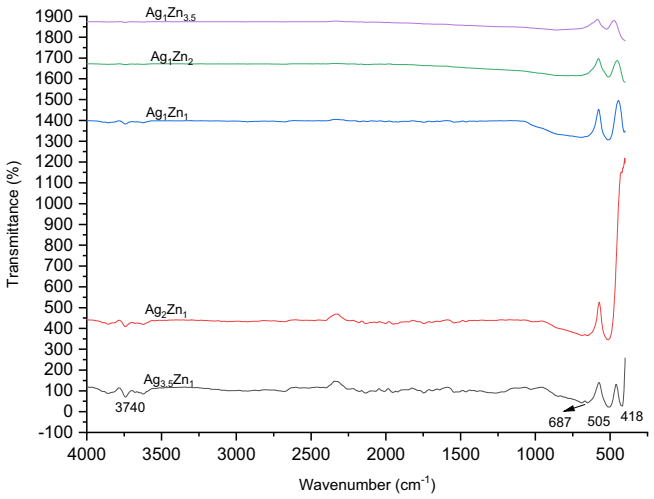

FIGURE 3 FTIR of Ag_1Zn_1, Ag_2Zn_1, Ag_1Zn_2, $Ag_{3.5}Zn_1$, and $Ag_1Zn_{3.5}$ heterostructures

505 cm^{-1} are attributed to ZnO.[39] The medium-weak broad-band at 687 cm^{-1} is due to the changes arising from the microstructure of Ag/ZnO.

3.4 | SEM analysis

The SEM images of the synthesized Ag/ZnO are presented in Figure 4. The result showed that the initial concentration of the precursors dictates the morphology and shape of the synthesized Ag/ZnO heterostructures. At ratio 1:1, the surficial morphology revealed mixed nanowire and nanoflakes. Fixing Ag content while increasing the Zn content revealed irregular rough edge nanoflakes. Similarly, fixing the Zn content, while increasing the Ag content showed interwoven nanowire with decreasing average diameter of the interwoven nanowire from ±4.72 to ±3.81 nm. The diameter was calculated using ImageJ™.[40]

3.5 | TEM and EDX analysis

The EDX analysis is presented in Figure 5. The result showed that obtained heterostructures are highly pure. The principal elements are Zn, Ag, and O. The overlapping of Cl was attributed to the machine.

The TEM image of sample Ag_1/Zn_2 is presented in Figure 6. The result showed that ZnO could diffuse into the lattice structure of Ag^0. The Ag atoms formed a spherical ring around ZnO, trapping the ZnO molecules, forming a shell. In addition, the TEM image also showed near-regular spherical shaped ZnO attached and covered by Ag^0.

3.6 | Batch Adsorption kinetics

The time-concentration profiles of MDR *E. faecium* removal as a function of initial MDR *E. faecium* concentration that ranged between 3.3 x 10^4 and 1.16 x 10^5 are presented in Figure 7. The

19447450, 2022, 6, Downloaded from https://aiche.onlinelibrary.wiley.com/doi/10.1002/ep.13925 by South African Medical Research, Wiley Online Library on [22/02/2026]. See the Terms and Conditions (https://onlinelibrary.wiley.com/terms-and-conditions) on Wiley Online Library for rules of use; OA articles are governed by the applicable Creative Commons License

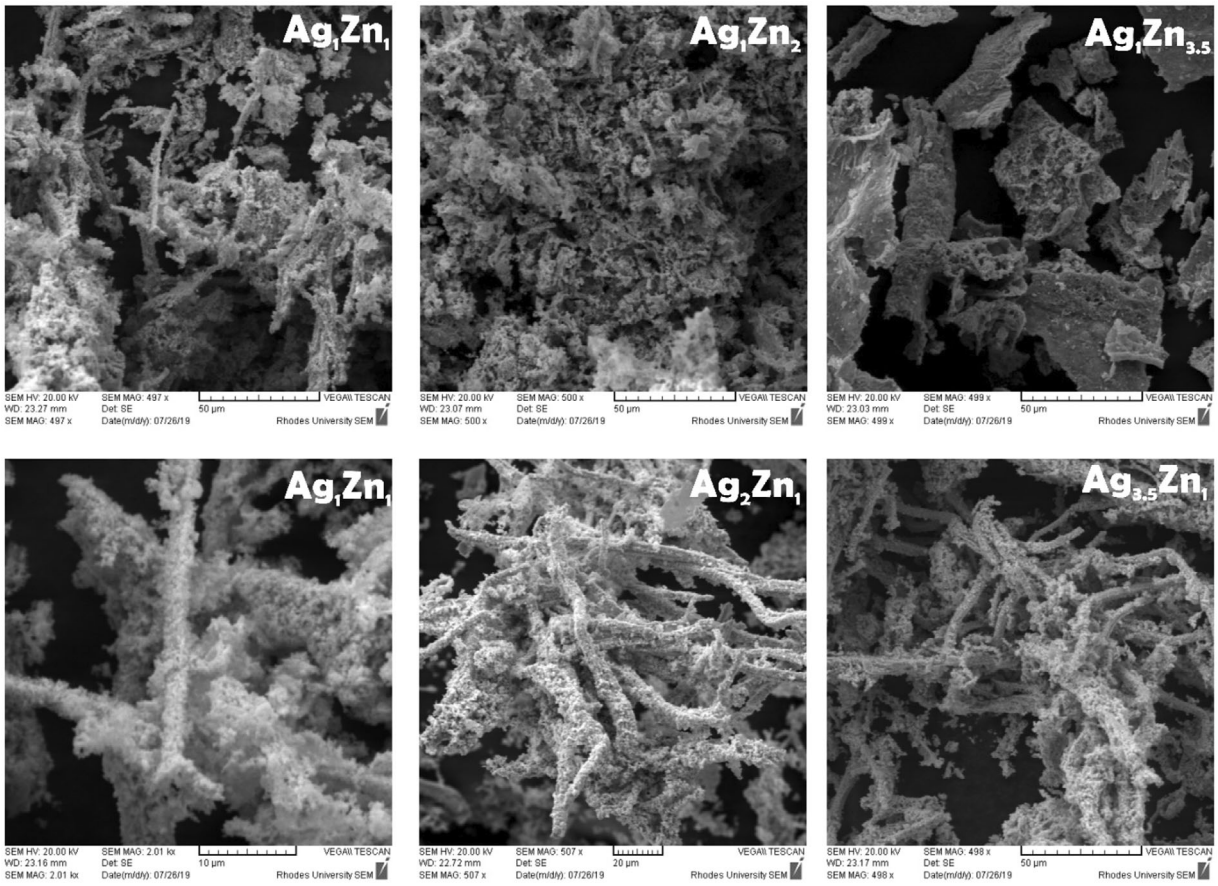

FIGURE 4 SEM micrographs of Ag_1Zn_1, Ag_2Zn_1, Ag_1Zn_2, $Ag_{3.5}Zn_1$, and $Ag_1Zn_{3.5}$

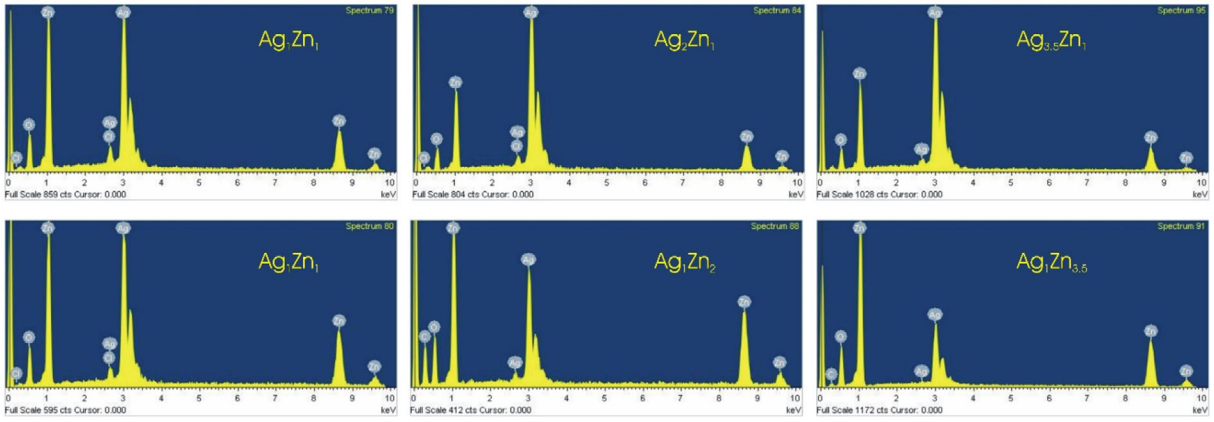

FIGURE 5 EDX analysis of the synthesized adsorbents

assessment of the time-concentration profiles of the five adsorbents (Ag_1Zn_1, Ag_2Zn_1, Ag_1Zn_2, $Ag_{3.5}Zn_1$, $Ag_1Zn_{3.5}$) showed that the removal of MDR *E. faecium* from tap water was initial concentration and time-dependent; thus, the adsorption rate and time of attainment of equilibrium varied. The reaction was almost instantaneous for all the adsorbents, as suggested by the sharp curves, especially at lower MDR *E. faecium* concentration. At higher MDR *E. faecium* initial concentrations, equilibrium was also achieved fast with higher removal magnitude (q_t). In this study, it is essential to note that adsorption equilibrium refers to the inabilities of MDR *E. faecium* to regrow. Therefore, the equilibrium that was achieved at less than 80 min was characterized by MDR *E. faecium* regrowth after 3 days. At time *t* greater than 90 min, no MDR *E. faecium* regrowth was observed even after 7 days.

To estimate the adsorption rate of Ag_1Zn_1, Ag_2Zn_1, Ag_1Zn_2, $Ag_{3.5}Zn_1$, $Ag_1Zn_{3.5}$ and other kinetic parameters, the time-concentration

19447450, 2022, 6, Downloaded from https://aiche.onlinelibrary.wiley.com/doi/10.1002/ep.13925 by South African Medical Research, Wiley Online Library on [22/02/2026]. See the Terms and Conditions (https://onlinelibrary.wiley.com/terms-and-conditions) on Wiley Online Library for rules of use; OA articles are governed by the applicable Creative Commons License

profiles obtained at different initial concentrations (3.3 x 10^4, 5.55 x 10^4, 8.55 x 10^4, 1.16 x 10^5) were fitted into the non-linearized pseudo-first-order[41] (Equation 6) and pseudo-second-order (Equation 7), where q_t and q_e (mg/g) are the amounts of MDR *E. faecium* uptake per mass of the adsorbents at equilibrium and at any time (minutes), respectively; k_1 (1/min) and k_2 (g/mg x min) are the rate constants. The fitness of the equations was observed using the Chi-square test (χ^2), where q_{t^*} is the calculated equilibrium at time *t*. A small value of χ^2 implies that the experimental data is similar to the calculated data.

$$q_t = q_e\left(1 - e^{-k_1 t}\right) \tag{6}$$

$$q_t = \frac{q_e^2 k_2 t}{1 + k_2 q_e t} \tag{7}$$

$$\chi^2 = \sum \frac{(q_t - q_{t*})^2}{q_{t*}} \tag{8}$$

The obtained data (Table 1) showed that adsorbents Ag_1Zn_1 and Ag_1Zn_2 were better fitted into the pseudo-first-order kinetic equation. The pseudo-first-order kinetic equation assumes that the adsorption of one ion (MDR *E. faecium*) occurs at one unoccupied adsorption site on the Ag_1Zn_1 and Ag_1Zn_2 adsorbents.[42] Whereas adsorbents Ag_2Zn_1, $Ag_{3.5}Zn_1$ and $Ag_1Zn_{3.5}$ followed the pseudo-second-order kinetic equation. The pseudo-second-order kinetic assumed that the rate-limiting step is chemosorption and depends on the adsorption capacity. The adsorption capacity followed similar trend for both kinetic equations. The adsorption capacity q_e increased with increasing concentration, the maximum q_e was 32.44 and 34.11 mg/g, for pseudo-first order and pseudo-second order, respectively.

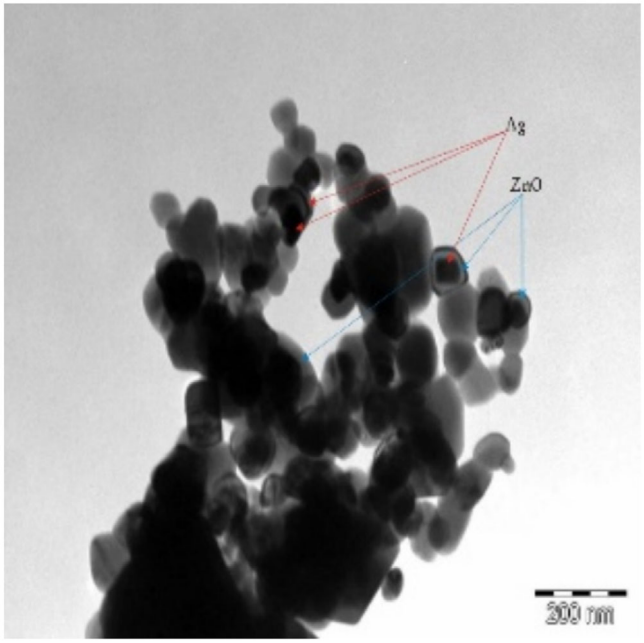

FIGURE 6 TEM image analysis of Ag_1Zn_2

3.7 | Electrical conductivity measurement

In order to gain an insight into the release of ions during batch adsorption kinetics, the electrical conductivity of the adsorbent/bacteria solution was monitored. The result was presented in Figure 8. This is important because, during bacteria membrane lysis, lipid peroxidation and K^+ release alter the ionic balance of the medium, thus, the conductivity determination. The results showed that the change in conductivity was minimal and ceased before 70 min. The highest change in conductivity was obtained with $Ag_{3.5}Zn_1$ (187 μS/cm), while the lowest was obtained using Ag_1Zn_1 adsorbent (161 μS/m). The physical contact between nanomaterial and bacteria is an essential mechanism for bacteria disinfection in water.[43] The slight change in the conductivity was attributed to the thick cell membrane of gram-positive bacteria. Gram-negative bacteria are susceptible to cell membrane rupture on mechanical mixing with adsorbents.[25] This is an indication that disinfection of the tap water may have been controlled by surface adsorption.

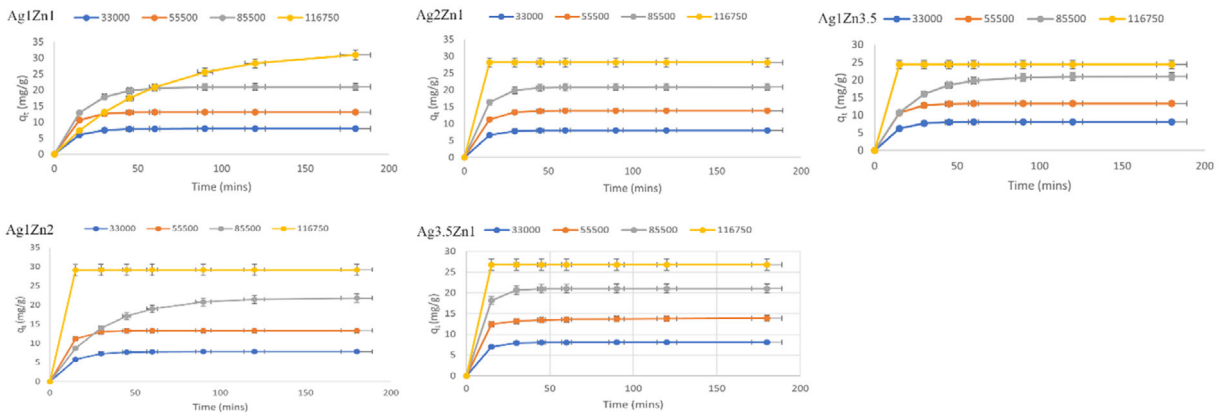

FIGURE 7 Adsorption kinetics characteristic curve of Ag_1Zn_1, Ag_2Zn_1, Ag_1Zn_2, $Ag_{3.5}Zn_1$, $Ag_1Zn_{3.5}$ adsorbents at different concentration

19447450, 2022, 6, Downloaded from https://aiche.onlinelibrary.wiley.com/doi/10.1002/ep.13925 by South African Medical Research, Wiley Online Library on [22/02/2026]. See the Terms and Conditions (https://onlinelibrary.wiley.com/terms-and-conditions) on Wiley Online Library for rules of use; OA articles are governed by the applicable Creative Commons License

TABLE 1 The obtained adsorption kinetic parameters for the removal of MDR *Enterococcus faecium*

Conc. (CFU/ml)	Pseudo first order			Pseudo second order		
Ag_1Zn_1	K_1	q_{e1}	χ^2	k_2	q_{e2}	χ^2
3.3×10^4	0.0932	7.9619	0.0073	0.0209	8.5191	0.0001
5.55×10^4	0.1102	13.1049	0.0094	0.0164	13.8879	0.0008
8.55×10^4	0.0634	21.0106	0.0065	0.0042	23.2239	0.0184
1.16×10^5	0.0172	32.4495	0.0762	0.0003	44.7168	0.0941
Ag_2Zn_1						
3.3×10^4	0.1177	8.0543	0.007	0.0316	8.4670	0.001
5.55×10^4	0.1128	9.3498	0.0082	0.0208	14.2090	0.0013
8.55×10^4	0.1018	20.8628	0.0056	0.0094	22.1474	0.001
1.16×10^5	1.2408	28.1422	0.1426	0.0031	30.9153	0.0171
Ag_1Zn_2						
3.3×10^4	0.0891	7.8191	0.035	0.0181	8.4720	0.0124
5.55×10^4	0.1221	13.3004	0.0178	0.0181	14.0674	0.0053
8.55×10^4	0.0340	21.8331	0.0133	0.0015	25.9174	0.028
1.16×10^5	0.4000	29.1753	0.0001	1.6115	29.1796	0.0001
$Ag_{3.5}Zn_1$						
3.3×10^4	0.1346	8.0586	0.0071	0.0399	8.4094	0.0013
5.55×10^4	0.1234	55.0047	0.9679	0.0373	14.0215	0.0011
8.55×10^4	0.1328	21.0373	0.0022	0.0163	21.8616	0.0001
1.16×10^5	1.0538	26.7882	0.0542	0.0064	29.8287	0.005
$Ag_1Zn_{3.5}$						
3.3×10^4	0.0966	8.1601	0.0047	0.0233	8.6541	0.003
5.55×10^4	0.1070	13.3247	0.0123	0.0151	14.1677	0.0018
8.55×10^4	0.0477	21.0285	0.0021	0.0027	23.9618	0.0082
1.16×10^5	1.7583	24.3596	0.3189	0.0014	34.1126	0.0276

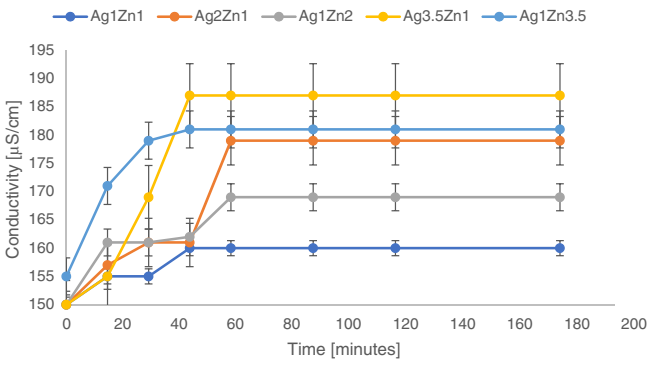

FIGURE 8 The change in conductivity during the removal of MDR *Enterococcus faecium* at 2.2×10^6 initial concentration with respect to time

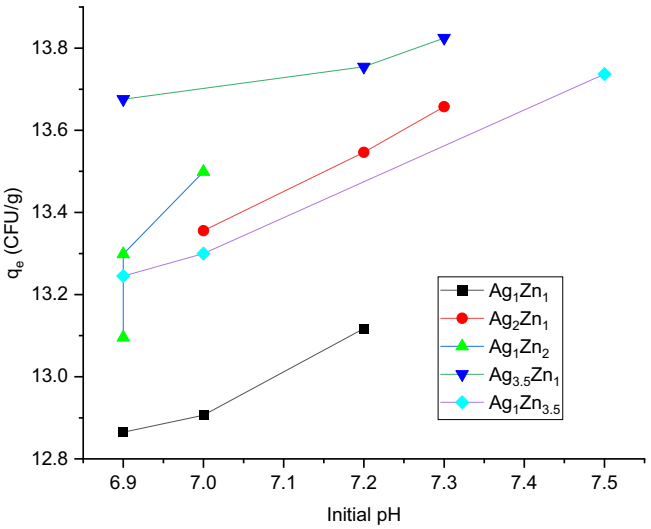

FIGURE 9 The effect of operating pH on the removal of MDR *Enterococcus faecium* from water

3.8 | Operating parameters

3.8.1 | Effect of operating pH

The result obtained for the effect of operating pH on the removal of *MDR E. faecium* is presented in Figure 9. The initial pH of the bacteria solution was adjusted to 5.2, 7.5 and 9.1. Gram positive bacteria are characterized by overall negative charge due to the phosphate group presence in teichoic acids attached to the peptidoglycan or to the underlying plasma membrane.[44] However, on *E. faecium* resistance acquisition,

19447450, 2022, 6, Downloaded from https://aiche.onlinelibrary.wiley.com/doi/10.1002/ep.13925 by South African Medical Research, Wiley Online Library on [22/02/2026]. See the Terms and Conditions (https://onlinelibrary.wiley.com/terms-and-conditions) on Wiley Online Library for rules of use; OA articles are governed by the applicable Creative Commons License

it is typified by positive charge.[45] The result showed that for all the absorbents (Ag_1Zn_1, Ag_2Zn_1, Ag_1Zn_2, $Ag_{3.5}Zn_1$, $Ag_1Zn_{3.5}$), increasing initial pH solution toward alkalinity was beneficial for the removal of MDR *E. faecium*. This is an indication of innersphere complexation.[46] This is attributed to the abundance of positively charge ions on the surface of the adsorbents at solution pH (5.2), which is less than the PZC, thereby causing repulsion between the gram-positive *MDR E. faecium* and the adsorbents. Above the initial solution pH (7.5 and 9.1) greater than the PZC, the adsorbents' surface is covered with a significant amount of negatively charged ions which attracts the gram-positive *MDR E. faecium* to the surface of the adsorbents. The trend of removal followed $Ag_{3.5}Zn_1 > Ag_1Zn_{3.5} > Ag_2Zn_1 > Ag_1Zn_2 > Ag_1Zn_1$. In general, the adsorbents used in this study caused solution equilibrium pH to approach neutral. The final pH was ≈6.9, 7.0 and 7.2 for all the adsorbents.

3.8.2 | Ionic strength

The effect of the ionic strength on the removal of *E. faecium* from tap-water is presented in Figure 10. The bonding of non-specifically adsorbed molecules is sensitive to change in ionic strength than specifically bonded molecules because electrolytes tend to form outer-sphere with the adsorbent.[47] The result showed that changes in ionic strength of the solution do not impact on the adsorption of MDR *E. faecium*, suggesting that the adsorption of MDR *E. faecium* was caused by inner sphere complexation. That is, the portion of MDR *E. faecium* in the outersphere is insignificant.

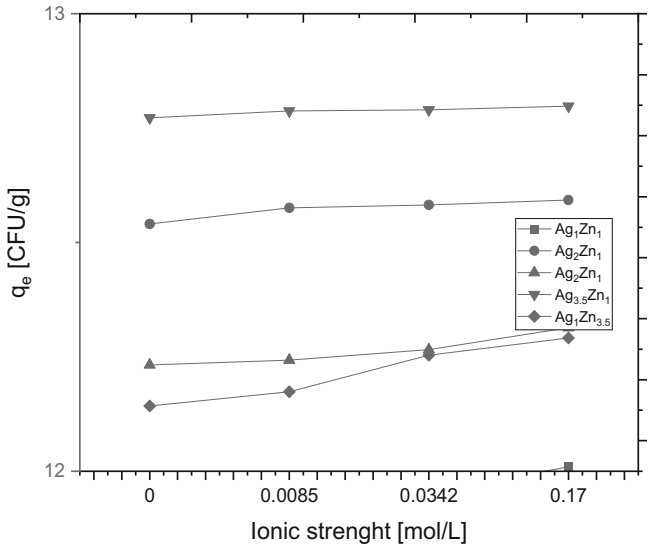

FIGURE 10 Effect of ionic strength on the removal of *Enterococcus faecium* from tap water

3.8.3 | Effect of anionic interference

The effect of anionic (carbonate and sulfate) interference on the removal of *E. faecium* from tap water is presented in Figure 11. The result showed that the removal of *E. faecium* from tap water increased with increase in anionic species concentration for all the adsorbents. The addition of the anions (sulfate and carbonate) caused the initial pH of the solution to increase from 6.0 to 7.8, 8.5 and 8.9 for 10 mg/L, 50 mg/L and 100 mg/L CO_3^{2-}, respectively. A similar trend in change in the initial solution pH was also observed with SO_4^{2-}. In aqueous solution, stimulated using Hydra/Medusa™, dissolved carbonate predominates as H_2CO_3 at pH <6.4, as CO_3^{2-} at pH > 10.5, and as HCO_3^- between pH range between 6.5 and 10.4, while SO_4^{2-} predominate as HSO_4^- at pH <2.1 and SO_4^{2-} at pH >2.1. Therefore, the reacting media contain abundant anions (HCO_3^-,SO_4^{2-}, and OH^-) that favors the adsorption of the MDR *E. faecium*. The increase in adsorption capacity was attributed to the cumulative negative cloud created on the adsorbents by the anions opposing the MDR *E. faecium* surface charge at the operating pH.

3.8.4 | Effect of cationic interference

The result obtained for the effect of cationic interference on the removal of MDR *E. faecium* from tap-water is presented in Figure 12. The result showed that the effect of Ca^{2+} ions on the removal of MDR *E. faecium* was beneficial for all the adsorbents except Ag_1Zn_1, while the addition of Mg^{2+} was unbeneficial for Ag_1Zn_1, Ag_1Zn_2, $Ag_1Zn_{3.5}$. Overall, the addition of the Ca^{2+} and Mg^{2+} ions did not alter the solution pH significantly; the initial solution pH after the addition of the cations at different concentration, was approximately 6.1. Therefore, the competitive effect for adsorption site caused by the cations during the adsorption of MDR *E. faecium* onto Ag_1Zn_1, Ag_1Zn_2, $Ag_1Zn_{3.5}$ adsorbents was significant, leading to lower adsorption capacity.

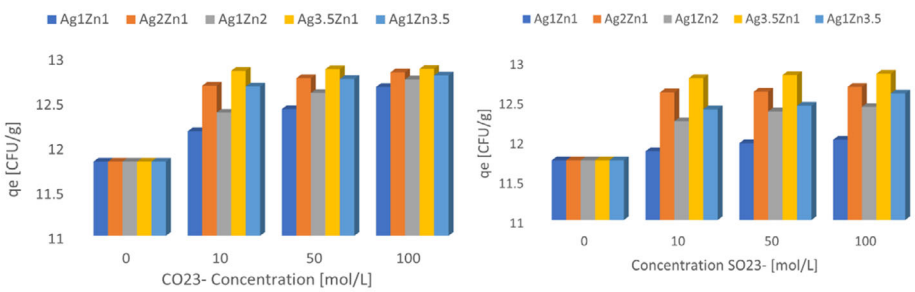

FIGURE 11 Effect of anionic interference (carbonate and sulfate)

19447450, 2022, 6, Downloaded from https://aiche.onlinelibrary.wiley.com/doi/10.1002/ep.13925 by South African Medical Research, Wiley Online Library on [22/02/2026]. See the Terms and Conditions (https://onlinelibrary.wiley.com/terms-and-conditions) on Wiley Online Library for rules of use; OA articles are governed by the applicable Creative Commons License

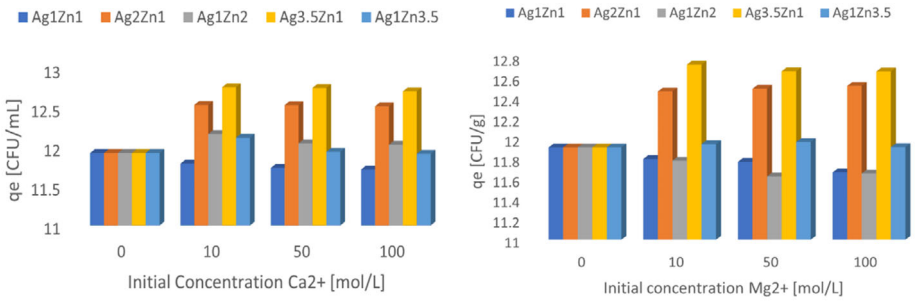

FIGURE 12 Effect of cationic interference Ca^{2+} and Mg^{2+}

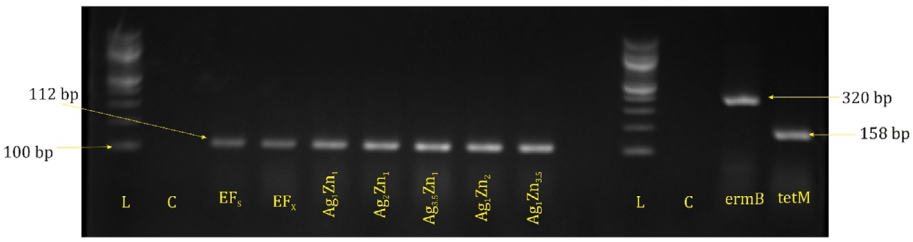

FIGURE 13 Gel electrophoresis image showing the presence of MDR *Enterococcus faecium* after 70 min treatments with the adsorbents, where C, EF_S and EF_X are the control, standard (DSM 20478) and isolated MDR *E. faecium*, respectively. The MDR *E. faecium* harbors resistance genes (ermB and tetM)

3.9 | Resuscitated cell integrity and antibiotic susceptibility test

The adsorbent used in this study possess bacteriostatic and bactericidal properties. The mechanism of action of these metals includes surface adsorption of bacteria on the adsorbent and poisoning of cell membrane via diffusion of the metal ions into the bacteria membranes, which may ultimately lead to DNA leakage and breakage. Gel electrophoresis is a powerful tool that can be employed to detect DNA breakage.[48] The breakage in DNA may be correlated with the change in the DNA size.[49] The image of the Gel electrophoresis of the resuscitated MDR *E. faecium* is presented in Figure 13. The result showed no change in MDR *E. faecium* DNA size of samples collected at 70 min. The sample time was chosen because this is the maximum time in which bacteria could regrow for all the adsorbents, at constant conductivity values. This result affirmed that the interaction of the adsorbents with MDR *E. faecium* did not cause irreparable damage to the genomic DNA at 70 mins reaction time and the resistance genes cassettes (*ermB* and *tetM*) are retained. This suggests that adsorption played primary role in the removal of the MDR *E. faecium* from the tap water.

3.10 | Reaction mechanism

The image obtained from the gel-electrophoresis showed that the size of the genomic DNA obtained for the standard, untreated and treated MDR *E. faecium* at time $t = 70$ min, were equal. The treated MDR *E. faecium* at time $t = 70$ min also retained its resistance genes. This is a strong indication that the removal of MDR *E. faecium* from the tap water was primary caused by the uptake of the MDR *E. faecium* onto the adsorbent and the adsorbent did not cause irreparable membrane damage. This agreed with our kinetic results.

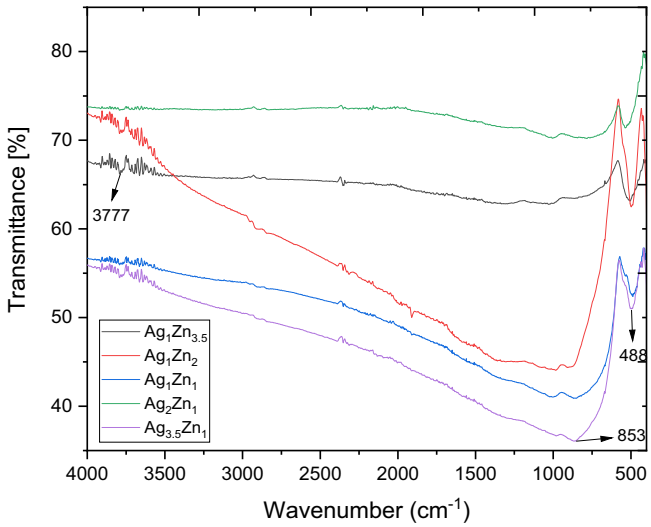

FIGURE 14 FTIR of MRD *Enterococcus faecium* laden adsorbents

The FTIR spectra of the *MDR E. faecium* laden adsorbents Ag_1Zn_1, Ag_2Zn_1, Ag_1Zn_2, $Ag_{3.5}Zn_1$, $Ag_1Zn_{3.5}$ were recorded between the range 4000 and 400 cm^{-1}, (Figure 14). The results showed a sharp, intense peak at 488 cm^{-1} representatives of all the adsorbents, likened to the peak at 418 cm^{-1} (Figure 3). The reduction in the functional group may cause shifting toward higher frequency in the IR spectrum; this may occur after adsorption of *MDR E. faecium* on the adsorbents. The new broad peak at 853 cm^{-1} which is peculiar to adsorbents Ag_1Zn_1,

19447450, 2022, 6, Downloaded from https://aiche.onlinelibrary.wiley.com/doi/10.1002/ep.13925 by South African Medical Research, Wiley Online Library on [22/02/2026]. See the Terms and Conditions (https://onlinelibrary.wiley.com/terms-and-conditions) on Wiley Online Library for rules of use; OA articles are governed by the applicable Creative Commons License

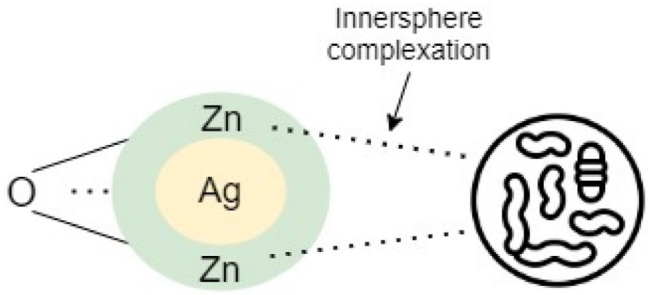

FIGURE 15 Adsorption mechanism of for the removal of MDR *Enterococcus faecium* from tap water

Ag_1Zn_2, and $Ag_{3.5}Zn_1$, was attributed to the adsorption site at the microstructural changes. The peak at 3777 cm^{-1} was slightly enhanced, suggesting an adsorption site at —OH group on the surface of the Ag/ZnO adsorbents. This suggests multiply sites of adsorption for the removal of *MDR E. faecium* from tap water.

The speciation diagram of the adsorbents constitutes showed that Ag^0 and Zn^{2+} predominant at the equilibrium pH as Ag^+ and, Zn^{2+}, $ZnOH^+$ and $Zn(OH)_2$, respectively. This would limit the coordination of Ag^0 to innersphere due to the lack of σ donor, whereas, the bonding with Zn^{2+} may coordinate via both inner and outersphere complexation (Figure 15). The more electronegative atom (oxygen) in the adsorbents would withdraw electron density, suggesting that the synthesized adsorbents would be available as $[AgZn]^+[OH]^-$ in the aqueous solution. The surface constituent of MDR *E. faecium* responsible for chemical bonding includes amino acids, sugar, and oligopeptides.

Therefore, the negatively charged OH— reactive site on the adsorbent is viable for the adsorption of the surface constituents (amino acids, sugar, oligopeptides) MDR *E. faecium* via innersphere complexation. This site is further enhanced in at pH greater than PZC. This supports our previous results in section 3.8.1.

4 | CONCLUSION

Different Ag/ZnO heterostructures, synthesized using the self-propagation combustion reaction, can be employed for the removal of MDR *E. faecium* from tap water. The concentration of the precursors dictates the microstructure of the adsorbents. However, no significant relationship was observed for the all the adsorbents with respect to the concentration of the precursors in the removal of MDR *E. faecium* from tap-water. The results showed that the removal of the MDR *E. faecium* was caused by surface adsorption onto the adsorbents and cell rupture was not observed up to 70 min reaction time. The maximum q_e (34.11 CFU/g) was obtained for $Ag_1Zn_{3.5}$. No significant relationship was observed for the all the adsorbents with respect to the concentration of the precursors in the removal of MDR *E. faecium* from tap-water. The adsorption of the MDR *E. faecium* onto the Ag/ZnO adsorbents was caused by inner-sphere complexation and initial solution pH and anionic interference affects the adsorption process.

Our results showed that the concentration of individual precursor greatly influenced the shape and morphology of the resulting Ag/ZnO composite. The morphology of the resulting composite has little impact on the removal of MDR *E. faecium*. However, the adsorption did not compromise the size of the extracellular genes of the MDR *E. faecium*, suggesting surface adsorption as the controlling mechanism.

AUTHOR CONTRIBUTIONS

Mike Ojemaye: Data curation (equal); investigation (equal); methodology (equal); project administration (equal); supervision (equal); validation (equal); visualization (equal); writing – original draft (equal); writing – review and editing (equal). **Omobola O Okoh:** Funding acquisition (lead); supervision (lead); validation (equal); writing – original draft (equal); writing – review and editing (equal). **Anthony Okoh:** Funding acquisition (lead); supervision (lead); writing – review and editing (equal).

FUNDING INFORMATION

The authors wish to thank the South Africa Medical Research Council and GMRDC, University of Fort Hare, South Africa for financial support.

CONFLICT OF INTEREST

The authors declare no conflict of interest.

DATA AVAILABILITY STATEMENT

Data are available on request.

ORCID

Eric T. Anthony https://orcid.org/0000-0002-0217-7585

REFERENCES

1. Ventola CL. The antibiotic resistance crisis—causes and threats. *P T J*. 2015;40:277-283.
2. O'Flaherty E, Borrego CM, Balcázar JL, Cummins E. Human exposure assessment to antibiotic-resistant *Escherichia coli* through drinking water. *Sci Total Environ*. 2018;616–617:1356-1364. doi:10.1016/j.scitotenv.2017.10.180
3. Seyedsayamdost E. *Sustainable Development Goals*, UN-Water; 2018. https://www.un.org/sustainabledevelopment/water-and-sanitation/
4. Han Z, An W, Yang M, Zhang Y. Assessing the impact of source water on tap water bacterial communities in 46 drinking water supply systems in China. *Water Res*. 2020;172:115469. doi:10.1016/j.watres.2020.115469
5. Barcina I, Lebaron P, Vives-Rego J. Survival of allochthonous bacteria in aquatic systems: a biological approach. *FEMS Microbiol Ecol*. 2006;23:1-9. doi:10.1111/j.1574-6941.1997.tb00385.x
6. Franz CMAP, Holzapfel WH, Stiles ME. Enterococci at the crossroads of food safety? *Int J Food Microbiol*. 1999;47:1-24. doi:10.1016/S0168-1605(99)00007-0
7. Roccaro P, Mancini G, Vagliasindi FGA. Water intended for human consumption—part I: compliance with European water quality standards. *Desalination*. 2005;176:1-11. doi:10.1016/j.desal.2004.11.010
8. Weiner LM, Webb AK, Limbago B, et al. Antimicrobial-resistant pathogens associated with healthcare-associated infections: summary of

19447450, 2022, 6, Downloaded from https://aiche.onlinelibrary.wiley.com/doi/10.1002/ep.13925 by South African Medical Research, Wiley Online Library on [22/02/2026]. See the Terms and Conditions (https://onlinelibrary.wiley.com/terms-and-conditions) on Wiley Online Library for rules of use; OA articles are governed by the applicable Creative Commons License

data reported to the National Healthcare Safety Network at the Centers for Disease Control and Prevention, 2011-2014. *Infect Control Hosp Epidemiol*. 2016;37:1288-1301. doi:10.1017/ice.2016.174
9. Behnke M, Hansen S, Leistner R, et al. Nosocomial infection and antibiotic use: a second national prevalence study in Germany. *Dtsch Arztebl Int*. 2013;110:627-633. doi:10.3238/arztebl.2013.0627
10. Hidron AI, Edwards JR, Patel J, et al. Antimicrobial-resistant pathogens associated with healthcare-associated infections: annual summary of data reported to the National Healthcare Safety Network at the Centers for Disease Control and Prevention, 2006–2007. *Infect Control Hosp Epidemiol*. 2008;29:996-1011. doi:10.1086/591861
11. Giannakis S, Le TTM, Entenza JM, Pulgarin C. Solar photo-Fenton disinfection of 11 antibiotic-resistant bacteria (ARB) and elimination of representative AR genes. Evidence that antibiotic resistance does not imply resistance to oxidative treatment. *Water Res*. 2018;143:334-345. doi:10.1016/j.watres.2018.06.062
12. Liu SS, Qu HM, Yang D, et al. Chlorine disinfection increases both intracellular and extracellular antibiotic resistance genes in a full-scale wastewater treatment plant. *Water Res*. 2018;136:131-136. doi:10.1016/j.watres.2018.02.036
13. Oladoja NA. Appropriate technology for domestic wastewater management in under-resourced regions of the world. *Appl Water Sci*. 2017;7:3391-3406. doi:10.1007/s13201-016-0495-z
14. Ain QU, Farooq MU, Jalees MI. Application of magnetic graphene oxide for water purification: heavy metals removal and disinfection. *J. Water Process Eng*. 2020;33:101044. doi:10.1016/j.jwpe.2019.101044
15. Anthony ET, Ojemaye MO, Okoh AI, Okoh OO. Potentials of low-cost methods for the removal of antibiotic-resistant bacteria and their genes in low budget communities: a review. *J Water Process Eng*. 2021;40:101919. doi:10.1016/j.jwpe.2021.101919
16. Kanchanapally R, Nellore BPV, Sinha SS, et al. Antimicrobial peptide-conjugated graphene oxide membrane for efficient removal and effective killing of multiple drug resistant bacteria. *RSC Adv*. 2015;5:18881-18887. doi:10.1039/c5ra01321f
17. Liu M, Zhu H, Zhu N, Yu Q. Vacancy engineering of BiOCl microspheres for efficient removal of multidrug-resistant bacteria and antibiotic-resistant genes in wastewater. *Chem Eng J*. 2021;426:130710. doi:10.1016/j.cej.2021.130710
18. Debnath A, Saha S, Li DO, et al. Elimination of multidrug-resistant bacteria by transition metal dichalcogenides encapsulated by synthetic single-stranded DNA. *ACS Appl Mater Interfaces*. 2021;13:8082-8094. doi:10.1021/acsami.0c22941
19. Mac Mahon J, Pillai SC, Kelly JM, Gill LW. Solar photocatalytic disinfection of E. coli and bacteriophages MS2, ΦX174 and PR772 using TiO_2, ZnO and ruthenium based complexes in a continuous flow system. *J. Photochem. Photobiol. B Biol*. 2017;170:79-90. doi:10.1016/j.jphotobiol.2017.03.027
20. Khatami M, Varma RS, Zafarnia N, Yaghoobi H, Sarani M, Kumar VG. Applications of green synthesized Ag, ZnO and Ag/ZnO nanoparticles for making clinical antimicrobial wound-healing bandages. *Sustain Chem Pharm*. 2018;10:9-15. doi:10.1016/j.scp.2018.08.001
21. Joe A, Park SH, Shim KD, et al. Antibacterial mechanism of ZnO nanoparticles under dark conditions. *J Ind Eng Chem*. 2017;45:430-439. doi:10.1016/j.jiec.2016.10.013
22. Tang S, Zheng J. Antibacterial activity of silver nanoparticles: structural effects. *Adv Healthc Mater*. 2018;7:1701503. doi:10.1002/adhm.201701503
23. Agnihotri S, Mukherji S, Mukherji S. Immobilized silver nanoparticles enhance contact killing and show highest efficacy: elucidation of the mechanism of bactericidal action of silver. *Nanoscale*. 2013;5:7328-7340. doi:10.1039/c3nr00024a
24. Elbourne A, Chapman J, Gelmi A, Cozzolino D, Crawford RJ, Truong VK. Bacterial-nanostructure interactions: the role of cell elasticity and adhesion forces. *J Colloid Interface Sci*. 2019;546:192-210. doi:10.1016/j.jcis.2019.03.050
25. Linklater DP, Baulin VA, Juodkazis S, Crawford RJ, Stoodley P, Ivanova EP. Mechano-bactericidal actions of nanostructured surfaces. *Nat Rev Microbiol*. 2021;19:8-22. doi:10.1038/s41579-020-0414-z
26. Di Mauro A, Farrugia C, Abela S, et al. Ag/ZnO/PMMA nanocomposites for efficient water reuse. *ACS Appl Bio Mater*. 2020;3:4417-4426. doi:10.1021/acsabm.0c00409
27. Song J, Sun G, Yu J, Si Y, Ding B. Construction of ternary ag@ZnO/TiO_2 fibrous membranes with hierarchical nanostructures and mechanical flexibility for water purification. *Ceram Int*. 2020;46:468-475. doi:10.1016/j.ceramint.2019.08.284
28. Sampaio MJ, Lima MJ, Baptista DL, Silva AMT, Silva CG, Faria JL. Ag-loaded ZnO materials for photocatalytic water treatment. *Chem Eng J*. 2017;318:95-102. doi:10.1016/j.cej.2016.05.105
29. Liu Y, Zhang Q, Xu M, et al. Novel and efficient synthesis of Ag-ZnO nanoparticles for the sunlight-induced photocatalytic degradation. *Appl Surf Sci*. 2019;476:632-640. doi:10.1016/j.apsusc.2019.01.137
30. Pant B, Park M, Kim H-Y, Park S-J. Ag-ZnO photocatalyst anchored on carbon nanofibers: synthesis, characterization, and photocatalytic activities. *Synth Met*. 2016;220:533-537. doi:10.1016/j.synthmet.2016.07.027
31. Hasan J, Webb HK, Truong VK, et al. Selective bactericidal activity of nanopatterned superhydrophobic cicada Psaltoda claripennis wing surfaces. *Appl Microbiol Biotechnol*. 2013;97:9257-9262. doi:10.1007/s00253-012-4628-5
32. Kumar R, Umar A, Kumar G, Nalwa HS. Antimicrobial properties of ZnO nanomaterials: a review. *Ceram Int*. 2017;43:3940-3961. doi:10.1016/j.ceramint.2016.12.062
33. Khan AU, Rahman A, Yuan Q, et al. Facile and eco-benign fabrication of Ag/Fe_2O_3 nanocomposite using Algaia Monozyga leaves extract and its' efficient biocidal and photocatalytic applications. *Photodiagnosis Photodyn Ther*. 2020;32:101970. doi:10.1016/j.pdpdt.2020.101970
34. Shannon RD. Revised effective ionic radii and systematic studies of interatomic distances in halides and chalcogenides. *Acta Crystallogr Sect A*. 1976;32:751-767. doi:10.1107/S0567739476001551
35. Oladoja NA, Anthony ET, Ololade IA, Saliu TD, Bello GA. Self-propagation combustion method for the synthesis of solar active Nano ferrite for Cr(VI) reduction in aqua system. *J Photochem Photobiol A Chem*. 2018;353:229-239. doi:10.1016/j.jphotochem.2017.11.026
36. Holzwarth U, Gibson N. The Scherrer equation versus the "Debye-Scherrer equation". *Nat Nanotechnol*. 2011;6:534. doi:10.1038/nnano.2011.145
37. Satdeve NS, Ugwekar RP, Bhanvase BA. Ultrasound assisted preparation and characterization of Ag supported on ZnO nanoparticles for visible light degradation of methylene blue dye. *J Mol Liq*. 2019;291:111313. doi:10.1016/j.molliq.2019.111313
38. Pandiyan N, Murugesan B, Arumugam M, Sonamuthu J, Samayanan S, Mahalingam S. Ionic liquid—a greener templating agent with Justicia adhatoda plant extract assisted green synthesis of morphologically improved Ag-Au/ZnO nanostructure and it's antibacterial and anticancer activities. *J Photochem Photobiol B Biol*. 2019;198:111559. doi:10.1016/j.jphotobiol.2019.111559
39. Liu H, Zhong L, Govindaraju S, Yun K. ZnO rod decorated with Ag nanoparticles for enhanced photocatalytic degradation of methylene blue. *J Phys Chem Solid*. 2019;129:46-53. doi:10.1016/j.jpcs.2018.12.040
40. Schneider CA, Rasband WS, Eliceiri, KW. NIG ImageJ: 25 years of image analysis. *Nature methods*. 2012; 671-675. doi:10.1038/nmeth.2089.
41. Lagergren S. About the theory of so-called adsorption of soluble substances. *Sven Vetenskapsakad Handingarl*. 1898;24:1-39.

19447450, 2022, 6, Downloaded from https://aiche.onlinelibrary.wiley.com/doi/10.1002/ep.13925 by South African Medical Research, Wiley Online Library on [22/02/2026]. See the Terms and Conditions (https://onlinelibrary.wiley.com/terms-and-conditions) on Wiley Online Library for rules of use; OA articles are governed by the applicable Creative Commons License

42. Li PHY, Bruce RL, Hobday MD. A pseudo first order rate model for the adsorption of an organic adsorbate in aqueous solution. *J Chem Technol Biotechnol*. 1999;74:55-59. doi:10.1002/(SICI)1097-4660(199901)74:13.0.CO;2-D
43. Heinlaan M, Ivask A, Blinova I, Dubourguier HC, Kahru A. Toxicity of nanosized and bulk ZnO, CuO and TiO_2 to bacteria Vibrio fischeri and crustaceans Daphnia magna and Thamnocephalus platyurus. *Chemosphere*. 2008;71:1308-1316. doi:10.1016/j.chemosphere.2007.11.047
44. Esmailzadeh H, Sangpour P, Shahraz F, Hejazi J, Khaksar R. Effect of nanocomposite packaging containing ZnO on growth of Bacillus subtilis and Enterobacter aerogenes. *Mater Sci Eng C*. 2016;58:1058-1063. doi:10.1016/j.msec.2015.09.078
45. Kumariya R, Sood SK, Rajput YS, Saini N, Garsa AK. Increased membrane surface positive charge and altered membrane fluidity leads to cationic antimicrobial peptide resistance in *Enterococcus faecalis*. *Biochim Biophys Acta - Biomembr*. 2015;1848:1367-1375. doi:10.1016/j.bbamem.2015.03.007
46. Rahnemaie R, Hiemstra T, van Riemsdijk WH. Inner- and outer-sphere complexation of ions at the goethite-solution interface. *J Colloid Interface Sci*. 2006;297:379-388. doi:10.1016/j.jcis.2005.11.003
47. Hsia TH, Lo SL, Lin CF, Lee DY. Characterization of arsenate adsorption on hydrous iron oxide using chemical and physical methods. *Colloids Surfaces A Physicochem Eng Asp*. 1994;85:1-7. doi:10.1016/0927-7757(94)02752-8
48. Drouin R, Gao S, Holmquist GP. Agarose gel electrophoresis for DNA damage analysis. *Technol Detect DNA Damage Mutat*. 1996:37–43. doi:10.1007/978-1-4899-0301-3_3
49. Sutherland JC, Monteleone DC, Trunk JG, Bennett PV, Sutherland BM. Quantifying DNA damage by gel electrophoresis, electronic imaging and number-average length analysis. *Electrophoresis*. 2001;22:843-854. doi:10.1002/1522-2683()22:53.0.CO;2-9

SUPPORTING INFORMATION

Additional supporting information can be found online in the Supporting Information section at the end of this article.

How to cite this article: Anthony ET, Ojemaye MO, Okoh OO, Okoh AI. Influence of different Ag/ZnO heterostructures on the removal efficiency of multidrug-resistant *Enterococcus faecium* harboring multiple resistance genes from tap water. *Environ Prog Sustainable Energy*. 2022;41(6):e13925. doi:10.1002/ep.13925

19447450, 2022, 6, Downloaded from https://aiche.onlinelibrary.wiley.com/doi/10.1002/ep.13925 by South African Medical Research, Wiley Online Library on [22/02/2026]. See the Terms and Conditions (https://onlinelibrary.wiley.com/terms-and-conditions) on Wiley Online Library for rules of use; OA articles are governed by the applicable Creative Commons License